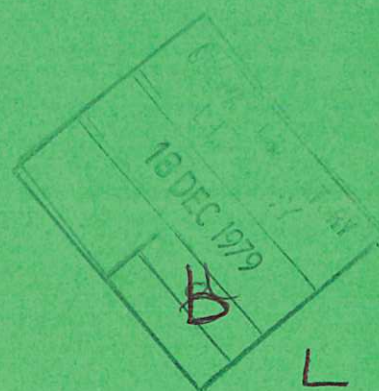UKAEA

Preprint

# THERMAL MOVING BOUNDARY PROBLEMS ARISING IN REACTOR SAFETY STUDIES

## R. S. PECKOVER

## CULHAM LABORATORY
Abingdon Oxfordshire

1979

# THERMAL MOVING BOUNDARY PROBLEMS ARISING IN REACTOR SAFETY STUDIES

by

R S Peckover

Culham Laboratory, Abingdon, Oxon. OX14 3DB, UK

## ABSTRACT

Stefan problems arise in a number of circumstances considered in reactor safety studies. For example, if after a hypothetical reactor core meltdown, debris penetrates through the bottom of the reactor vessel it will begin to melt into the material beneath. The maximum volume to which the resulting melt pool grows can be examined in a first approximation by assuming the pool grows hemispherically. At early times when the pool temperature can change rapidly, the Whipple equation is appropriate. At later times when the thermal conduction front in the solid broadens and the pool advance slows, an isotherm migration formulation is convenient. On the basis of suitable choices to approximate the temperature profile in the vicinity of the melt front, one can reduce the partial differential equations describing the system to an ordinary differential equation for the melt front which represents its temporal development well. These approximations can be easily generalised to model the asymmetric growth of pools in several dimensions. In the hemispherical case, satisfactory algebraic estimates of maximum pool size can be obtained. Computer studies have been carried out for a wide range of Stefan numbers to see how robust the approximations are.

A related problem concerns the stability of the melt front against the development of ripples or fingering. A linear analysis for a plane interface indicates that spatially localised modes are stable.

# 1. INTRODUCTION

A 'Stefan problem' in heat transfer is one in which a phase boundary is not fixed in space but moves as one phase changes into another; locating the position of the phase boundary as a function of time is an implicit part of the problem. The melting of ice in contact with water is the archetypal Stefan problem, studied by Stefan himself [1].

In a nuclear reactor under normal operation the location of solid/liquid interfaces is predetermined. However in the conceivable, but highly unlikely, event of a reactor core becoming significantly overheated then some part of the core might become molten, and the hot material might come in contact with core support structures or the bottom of the reactor vessel. In reactor safety studies such hypothetical events are examined and their consequences assessed to ensure that hot core material (which is heat producing because of the fission products it contains) comes to rest in a satisfactory manner. Clearly Stefan problems arise; for example overheated core material sitting on a steel strut could melt some of the steel, and it is useful to know how fast the melting front advances and what combinations of high temperature of core material and thickness of steel will result in complete liquefaction of the strut. A mathematical problem which arises from considering molten steel overlying the solid steel of a partially melted horizontal plate is the stability of the melting front shape against localized spatial perturbations. This is considered in §6.

If, after a hypothetical core meltdown, debris falls to the bottom of the reactor vessel and then melts through, it will begin to melt into the material beneath. This may be natural bed rock or a 'sacrificial' material placed there against this eventuality. In either case it is necessary to estimate how large a molten pool of material will grow. We consider here only the case where the molten debris and the sacrificial material are miscible. Sections 2 - 5 are concerned with the growth of such a melt pool.

Other moving boundary problems may arise earlier in a postulated accident sequence. Film boiling of the liquid coolant on overheated fuel pins is a complicated Stefan problem - the water/steam interface in aqueous film boiling is known to be a rapidly fluctuating highly irregular surface. Some kinds of fuel pins consist of a cylinder of high melting point ceramic fuel encased in steel; under what circumstances does the clad melt before the fuel does? If molten fuel has escaped from a fuel pin and is flowing down the outer surface of some steel structure, how quickly does the fuel freeze? (The flow of molten wax down the solid perimeter of a candle must have been a familiar

realisation of this problem prior to the widespread use of electric lighting). In all such problems the ability to predict in awkward geometries the progress of melting or freezing fronts is of practical utility.

The accuracy to which the answer is required depends on carrying out some sort of error analysis to see which parts of a sequence of events contribute most to the end result, in terms of time scale and magnitude. For the molten pool problem considered in sections 2 - 5, accurate results are needed for detailed design studies, but simpler approximations are adequate for parametric material surveys.

## 2. GROWTH OF A MELTPOOL

If it is postulated that a meltpool has formed beneath the reactor vessel in the solid substrate with which the molten debris is miscible, then the energy balance is

$$- F_{up} + Q(t) = \int_V \frac{\partial}{\partial t}\left[\rho_\ell c_\ell T\right] dV' + \rho L \int_\Omega \underline{u} \cdot d\underline{S} - k \int_\Omega \nabla T \cdot d\underline{S} \qquad (2.1)$$

| ↑ | ↑ | ↑ | ↑ | ↑ |
|---|---|---|---|---|
| Heat Transfer Upwards to Coolant (1) | Decay Heat Source (2) | Change in Pool Temperature (3) | Advance of Melting Front (4) | Thermal Conduction into Bed (5) |

(see Fig. 1)

Here in the solid phase, $\rho$ is the density, $L$ is the latent heat of fusion and $k$ is the thermal conductivity. In the pool $\rho_\ell$ and $c_\ell$ are the density and specific heat of the liquid phase. The pool volume is $V$ and its lower surface is denoted by $\Omega$. For conservative (over) estimates of pool growth the upward heat transfer can be ignored and term (1) is set to zero. The pool is consequently taken to have an adiabatic upper lid. The decay heat source $Q(t)$ is the integral of a heat source density depending on the distribution of the fission products within the pool. However the distribution of heat flux along $\Omega$ depends mainly on the shape and size of the pool through their influence on convective motions in the pool, and depends only weakly on the actual distribution of heat sources within the pool volume. The temperature is represented by $T(\underline{r},t)$.

The quantities of interest are the shape and size of the pool when it reaches its maximum extent and the time it takes to do so. Hence it is the location of the melting front as a function of time which is required. The temperature distribution within the solid substratum is only of subsidiary interest in this application. The size of the meltpool can be examined in a first approximation by assuming that the pool grows as a hemisphere, using a mean heat transfer coefficient from the turbulently convecting pool. §3 and §4 are concerned with this model. To model the changes in aspect ratio of the pool properly, a full two-phase multi-dimensional formulation is required. Nevertheless very useful indications can be obtained by assuming the pool is ellipsoidal in shape and allowing both the scale and aspect ratio of the pool to evolve in time, coupled with the Fourier equation in the solid substratum. Details of results from this approach have been discussed elsewhere [2].

## 2.1  Heating Source Term

After the shutdown of a nuclear reactor, the reactor is no longer critical and the chain reactions stop.  Nevertheless heat continues to be produced as a result of the radioactive decay of the fission products generated by the nuclear reactions.  Immediately after shut down, the decay heat $Q(t)$ is a few per cent of the nominal reactor power $Q_o$ when in normal operation, and $Q(t)$ rapidly falls to less than $\frac{1}{2}\%$ of $Q_o$ within a week or so.  It has been found [3] that the decay heat $Q$ can be expressed in the functional form

$$Q(t) = \hat{Q}(t) - \hat{Q}(t+t_q) \qquad (2.2)$$

where $t_q$ is the irradiation time i.e. the mean time that the fuel has spent under normal operation prior to shutdown, and t is the time since shutdown.

If one writes $\qquad Q(t) \equiv Q_o f(t) \qquad (2.3)$,

then the functional form for $f(t)$, the decay heating function, is

$$f(t) = f_o(t^{-\alpha} - [t+t_q]^{-\alpha}) \qquad (2.4)$$

where $\alpha = \frac{1}{5}$ according to Way and Wigner [3].  A conservative estimate which envelopes modern data is $\alpha = \frac{1}{4}$.

The total decay heat generated up to time t is $\int_o^t Q(t')dt'$ which can be conveniently expressed as $Q_o\tau(t)$ where

$$\tau(t) = \int_o^t f(t')dt' \qquad (2.5).$$

$\tau$ is the equivalent number of full power reactor-seconds and is the measure of total decay heat used here.  f and $\tau$ are sketched in figure 2.  $\tau$ is bounded as $t\to\infty$ by $\frac{1}{1-\alpha} f_o t_q^{(1-\alpha)} \equiv \tau_\infty$.  Note that f is dimensionless and $\tau$ has dimensions of time.

## 2.2  Characteristics of Pool Growth

Four temporal phases can be distinguished for pool growth:

(i)  an early period when the pool temperature can change rapidly;  the movement of the melting front, though rapid, is limited by the thermal resistance of the boundary layer of the pool (the sum of terms (4) and (5) in (2.1) is bounded, so term (3) is significant).

(ii) a period when the pool is close to its melting point and the melting

2.2

front is advancing rapidly with the thermal leakage ahead of the front acting as preheating of the cold bed. (Term (3) in (2.1) is negligible and term (5) $\approx \rho c \Delta T \int \underline{u} . d\underline{S}$ where c is the specific heat of the solid and $\Delta T$ is difference between the melting temperature and the ambient temperature in the solid phase far from the pool).

(iii)  a period when the thermal conduction front broadens and the melting front slows.  The maximum pool size is reached at the end of this period.

(iv) a final period in which as the decay heating function continues to decrease, the pool shrinks.

Fig. 3 shows schematically the evolution of pool volume and pool temperature.

# 3. RADIAL GROWTH OF A HEMISPHERICAL MELTPOOL

The main characteristics of the growth of a meltpool can be examined by concentrating on a radial model in which the pool grows as a hemisphere whose radius is a function of time. Consequently the following assumptions are introduced; (i) the pool is hemispherical, of radius $R_o(t)$; (ii) the top surface of the pool is an 'insulated lid'; this forces all the heat being generated either to remain in the pool or be conducted into the bed; (iii) the pool is well mixed by turbulence and has essentially a uniform temperature $T_p$, together with a thermal boundary layer adjacent to the melting front which is at temperature $T_1$; (iv) the heat transfer coefficient from the pool to the melting front is independent of position on the melting front, and so is a mean heat transfer coefficient. These assumptions are discussed further elsewhere [2]. Fig. 4 illustrates the model.

## 3.1 Stage I

At early times, the pool grows rapidly, with negligible 'thermal leakage', which means that heat conducted into the bed is soon absorbed back into the pool by the advancing melting front (see §3.2 below). The energy balance equation 2.1 can thus be written approximately as

$$Q_o f = \rho c V \dot{T}_p + \rho (L + c \Delta T) \dot{V} \tag{3.1}$$

indicating that all the heat generated goes either into pool growth or into raising the pool temperature above its melting point. It is convenient to introduce a length scale b defined by

$$b = Q_o / 2\pi k (\Delta T) \tag{3.2}$$

This is the radius of the hemisphere which in equilibrium would be able to conduct away the full reactor power $Q_o$. Defining the non-dimensional radius $R_o(t)$ by $R_o = r/b$ and the non-dimensional pool temperature $\theta_p(t)$ by

$$\theta_p = (T_p - T_o)/\Delta T \tag{3.3}$$

we can re-cast (3.1) as

$$\kappa.bf = \tfrac{1}{3} \theta_p (R_o^3 - R_*^3) + R_o^2 (1 + s^{-1}) \dot{R}_o \tag{3.4}$$

in which S is the Stefan number $c(\Delta T)/L$, and $R_*$ is the dimensionless initial

3.1

radius of the pool, weighted to allow for the different values of thermal capacity in the bed material and the initial pool material. Note that $R_o(t) > R_o(0) > R_*$ and that b is much larger than the maximum pool radius $r_m$ (typically b $\sim$ 10 km, $r_m$ $\sim$ 10 m).

The heat used to advance the melting front is transmitted from the bulk of the pool through the thermal boundary layer within the pool and this process can be characterised by a heat transfer coefficient. This leads to

$$\rho c (1 + S^{-1}) \dot{R}_o = \beta (\theta_p - 1) \tag{3.5}$$

where $\beta$ is a scaled heat transfer coefficient. It is a function of the size, temperature and thermophysical properties of the pool, via correlations involving Grashof and Prandtl numbers.

Since t is the only independent variable in (3.4) and (3.5), one may write $\dot{\theta}_p = \dot{R}_o (d\theta_p/dR_o)$, which, when combined with (3.4) and (3.5) leads to the Whipple equation [2]

$$\frac{d\theta_p}{dR_o} = \frac{3(1 + S^{-1})}{(R_o^3 - R_*^3)} \left( \frac{kbf(t)}{\beta.(\theta_p-1)} - R_o^2 \right) \tag{3.6}$$

which is a first order ordinary differential equation for $\theta_p$ in terms of $R_o$ with a strongly non-linear right hand side. The corresponding time is obtained from (3.5), written in the form $dt = dR_o \rho c (1+S^{-1})/[\beta.(\theta_p-1)]$. The solution of such an equation is straightforward using O.D.E. packages currently available. Fig. 5 shows a typical result for $\theta_p(t)$. The mean pool temperature falls, to be quite close to the melting point within $\sim$ 1% of the time that it takes for the pool to reach its maximum size. The result is insensitive to the available choice of initial pool temperature since the initial heat content of the pool inevitably becomes a small fraction of that in the pool after only a few minutes.

Thus for later stages of pool growth it is permissible to assume that all the heated generated is transmitted instantaneously to the melting front, and this enables what is properly considered as a two-phase Stefan problem to be reduced to a one-phase Stefan problem. The delay in this transmission, introduced at early times by the rise and fall of the pool temperature, can be compensated for by an appropriate small modification in the time-dependence of f(t).

## 3.2   Stage II

In stage II, when the transient involving the pool temperature has decayed, the front is still moving rapidly.  The Fourier equation in the frame of the melting front can be written as

$$\frac{\partial y}{\partial t} = u\frac{\partial y}{\partial x} + \kappa \frac{\partial^2 y}{\partial x^2} \tag{3.7}$$

where $y = r\theta$ and $u = \dot{r}_o$.  This has a solution of the form

$$\theta = \frac{r_o}{r} e^{\frac{-ux}{\kappa}} \tag{3.8}$$

provided $\frac{\partial y}{\partial t}$ can be neglected, which is the case if (i) $u \gg \frac{\kappa}{r_o}$ and (ii) $\dot{u}x \ll u^2$.  The first condition requires that the front should be moving much faster than a 'thermal diffusion speed'.  The second condition implies that the velocity is changing slowly.  Since at a distance $x \sim \frac{3\kappa}{u}$ ahead of the front, $\theta$ would be $\sim 0.05$, $\dot{u} \leqslant u^3/3\kappa$ is a sufficiently slow rate of change.

Solution (3.8) is here called the 'fast melting front solution'.  In the neighbourhood of the front it has the exponential profile $\theta = e^{\frac{-ux}{\kappa}}$ of the asymptotic solution for a plane profile (since $u \gg \frac{\kappa}{r_o}$), and the flux at the melting front into the bed is given by

$$-k\,\Delta T\,\frac{\partial \theta}{\partial x}\bigg|_{x=0} = \rho c\,(\Delta T).u \tag{3.9}$$

Hence the energy balance equation (2.1) becomes at this stage

$$Q_o f = 2\pi r_o^2 \rho\,(L + c\Delta T)\,u \tag{3.10}$$

where the r.h.s. of (3.10) is identical with the second term on the r.h.s. of (3.1) This can be integrated directly to give

$$r_o^3 = \left[\frac{b^3}{1+s}\right]\frac{\tau}{t_N} \tag{3.11}$$

where the time scale $t_N = 2\pi\rho L b^3 / (3Q_o)$ (3.12)

which is the number of full reactor-seconds required to generate the latent heat of melting for a hemisphere of bed material of radius b.  As we shall see, it is very much larger than the time $t_m$ at which the maximum size of the pool is reached (typically $t_m \sim 10^8$s, $t_N \sim 10^{15}$s).  Equation (3.11) contains no constant of integration since we may take $r_o \simeq 0$, when t=0 for the initial pool size is small, compared with the maximum pool size $r_m$.

## 3.3  Stage III

This stage occupies the period between the time when the fast melting solution of §3.2 is valid and the time of pool maximum radius. Within the bed material the Fourier equation holds, and can be written in the frame of reference of the melting front as

$$\frac{\partial \theta}{\partial t} = \left( u + \frac{2\kappa}{r} \right) \frac{\partial \theta}{\partial x} + \kappa \frac{\partial^2 \theta}{\partial x^2} \qquad (3.13)$$

The Stefan condition at the melting front is

$$Q_o f = 2\pi r_o^2 k \Delta T \left( \left. \frac{-\partial \theta}{\partial x} \right|_{x=0} \right) + 2\pi r_o^2 \rho L \dot{r}_o \qquad (3.14)$$

where $x = r - r_o(t)$. Also $\theta = 1$ at the melting front.

There are a number of ways in which this Stefan problem can be handled numerically [4]; a method giving satisfactory results and good agreement with test problems is the Isotherm Migration Method [5, 6], which is the basis for the ISOTHM code in radial co-ordinates [2, 7]. Fig. 6 shows a typical set of isotherms produced by a run of ISOTHM for basalt with S $\sim$ 2. The bottom isotherm shown is that for the melting front, and at the time of pool maximum the isotherms adjacent to the front are almost horizontal, indicating that they too have only a small propagation speed at that time. The non-dimensional forms of the equations solved in ISOTHM are

$$\frac{\partial R_o}{\partial \sigma} = \frac{1}{3} \left[ \frac{f(t)}{R_o^2} + \left( \frac{\partial R}{\partial \theta} \right)_{R=R_o}^{-1} \right] \qquad (3.15)$$

for the Stefan condition and

$$S \frac{\partial R}{\partial \sigma} = \frac{1}{3} \left[ \frac{\partial^2 R}{\partial \theta^2} \left( \frac{\partial R}{\partial \theta} \right)^{-2} - \frac{2}{R} \right] \qquad (3.16)$$

for the Fourier equation where $\sigma \equiv t/t_N$. For a given decay heat function $f(t)$, these equations depend on only two parameters - the Stefan number S and the scaling time $t_N$. When $f(t)$ has the form given by (2.4) with $\alpha = \frac{1}{4}$, fig. 7(a) shows the dependence of the (dimensionless) maximum pool radius $R_m$ on S and $t_N$ and fig.7(b) shows the corresponding $t_m$.

In investigating a range of possible materials for beds beneath reactors of different nominal powers $Q_o$, it is convenient to be able to estimate $R_m$ and the corresponding $t_m$ without recourse to solving the partial differential equations (3.17, 3.18) or their equivalents.

The following section (§4) is concerned with estimating $R_m$ and $t_m$ in any particular case, with less expenditure in computer time.

# 4. APPROXIMATE METHODS FOR THE ONE-PHASE RADIAL STEFAN PROBLEM

4.1 By establishing two time-dependent upper bounds for the radius of a growing melt pool, a simple upper bound for the maximum pool radius can be obtained.

To obtain closer estimates of the maximum pool radius, two different approximate profiles for the temperature in the bed are derived heuristically and the corresponding evolution of the pool compared with results from ISOTHM.

## 4.2 A Simple Upper Bound

The 'fast melting front' solution discussed in §3.2 always exceeds the true solution, since the growing thermal boundary layer in the bed restricts the advance of the front. Defining

$$a^3 \equiv b^3 t_N^{-1} (1+S)^{-1} \qquad (4.1)$$

we can express eq.(3.11) as

$$r_o(t) = a\tau^{1/3} \qquad (4.2)$$

On the other hand the minimum quantity of heat which will be conducted away from a stationary pool of radius $r_o$ is $2\pi r_o^2 \left(-\kappa \frac{\partial T}{\partial r}\right)_{r=r_o}$ i.e. $2\pi k (\Delta T) r_o$ since $\theta = r_o/r$ in equilibrium. The heat generated must exceed the minimum requirement while the front is advancing. Thus $Q_o f(t) > 2\pi k (\Delta T) r_o$, and a second bounding curve for the position of the advancing front is

$$r_o(t) = bf \qquad (4.3)$$

Now (4.2) is a monotonic increasing function, whereas (4.3) is monotonic decreasing for decay heat functions of the form discussed in §2. Hence a simple upper bound is given by their intersection $r_B$ which occurs when $t=t_B$ satisfies

$$\tau(t_B)/t_N = (1+S)f^3(t_B) \qquad (4.4)$$

Figs. 8(a, b and c) and Table 1 give $(r_B, t_B)$ for different values of S for f of the form (2.4) with $\alpha=\frac{1}{4}$. For small S, $t_B$ is underestimated by $\sim 10\%$, whereas $r_B$ is overestimated by 30%. For large S, $t_B$ is overestimated by $\sim 40\%$, whereas $r_B$ is overestimated by $\sim 75\%$. For more general monotonically decreasing decay heat functions, this indicates that $r_B$ may be an overestimate by as much

4.1

as a factor of 2 and $t_B$ may be inaccurate to $\sim \pm 50\%$. The solution of (4.4) for $t_B$ is straightforward; there is only one root, and the forms of $\tau$ and $f$ are explicitly known, either analytically or in tabular form, with interpolation rules. With *regula falsi* [8], no more than 10 function evaluations would be required to obtain $t_B$ to 3 significant figures, giving $r_B$ to the same accuracy.

## 4.3 The Exponential Ansatz

From the arguments given in §4.2, the maximum pool radius will satisfy the simultaneous equations

$$\left. \begin{array}{l} r_o(t) = \lambda a \tau^{1/3} \\[2mm] r_o(t) = \mu b f \end{array} \right\} \tag{4.5}$$

when $t = t_m$ the time of pool maximum for some values of $\lambda$ and $\mu$ in the range $(0, 1)$. The simple upper bound obtained in §4.2 corresponds in these co-ordinates to $r_B \Longleftrightarrow (\lambda_B, \mu_B) = (1.1)$

From (3.15), at pool maximum $r_o^2 \frac{\partial \theta}{\partial r}|_{r=r_o} + bf = 0$, so that $r_m^2 = -bf(t_m) \frac{\partial \theta}{\partial r}|_{r=r_o}, \; t=t_m$. Determination of $\mu$ thus depends on evaluating the gradient $\frac{\partial \theta}{\partial r}$ in the bed at the melting front.

The energy balance equation can be written as

$$r_o^3 (1+G) = a^3 \tau \tag{4.6}$$

where $G$ is the ratio of enthalpy in the bed to that in the pool. Hence $\lambda = (1+G)^{-1/3}$, and determination of $\lambda$ depends on evaluating $G$. Thus $\mu$ depends on a local property in the vicinity of the melting front, whereas $\lambda$ depends on an integral property of the whole temperature profile.

In the vicinity of the melting front (where $\theta = 1$), eq.(3.13) becomes approximately,

$$\left( u + \frac{2\kappa}{r_o} \right) \frac{\partial \theta}{\partial x} + \kappa \frac{\partial^2 \theta}{\partial x^2} \simeq 0 \tag{4.7}$$

since $\frac{\partial \theta}{\partial t} \approx 0$ and $r \approx r_o$ when $\frac{x}{r_o} \ll 1$. This suggests as an approximate profile, the exponential Ansatz

$$\theta = \exp(-x/\delta(t)) \tag{4.8}$$

where

$$\frac{1}{\delta(t)} = \frac{u}{\kappa} + \frac{2}{r_o} \tag{4.9}$$

with $u = \dot{r}_o$. This profile $\to 0$ as $x \to \infty$, and gives $\theta = \exp\left(\frac{-ux}{\kappa}\right)$, the fast 'plane' melting front solution, when $u \gg \frac{\kappa}{r_o}$. From (4.8) $\frac{\partial \theta}{\partial x} = -\frac{1}{\delta}$ when $x = 0$, so that $\delta$ may be interpreted as the thickness of the thermal boundary layer within the front. Another important property of (4.8) is that $\delta$ is finite as $u \to 0$, which is obviously true in reality.

Insertion of (4.8) in (3.15) and into (3.16) as $R \to R_o$ gives

$$\frac{u}{\kappa} = S\left(\frac{bf}{r_o^2} - \frac{1}{\delta}\right) \tag{4.10}$$

$$\frac{u}{\kappa} = \left(\frac{1}{\delta} - \frac{2}{r_o}\right) \tag{4.11}$$

Hence at pool maximum

$$r_o = 2\delta = \frac{1}{2}bf \tag{4.12}$$

The enthalpy ratio $G = \left(\frac{3S}{1+S}\right)\left(2\left[\frac{\delta}{r_o}\right]^3 + 2\left[\frac{\delta}{r_o}\right]^2 + \left[\frac{\delta}{r_o}\right]\right)$ when $\theta$ has the profile (4.8), which reduces to $\frac{15}{4}\left(\frac{S}{1+S}\right)$ when $\delta = \frac{1}{2}r_o$.

Thus the pool maximum $r_A$ as estimated using the exponential Ansatz corresponds to

$$\left(\lambda_A, \mu_A\right) = \left(\left[\frac{1+S}{1+\frac{19}{4}S}\right]^{1/3}, \frac{1}{2}\right) \tag{4.13}$$

where the time of pool maximum $t_A$ satisfies

$$\tau/t_N = \frac{1}{8}\left[1+\frac{19}{4}S\right]f^3 \tag{4.14}$$

A comparison between the results from this approximation and those from the

ISOTHM code are given in Table 1. The estimate of the radius $r_A$ is good to 2.3% for $4 \times 10^{-2} < S < 10^2$, while the estimate of the time $t_A$ varies from being very satisfactory for large S to being much worse than $t_B$ for small S. Fig. 9 shows the temperature profile for $\theta$ as calculated by ISOTHM for a range of different values of $t_N$ when S is large, i.e. latent heat is negligible; the exponential profile is clearly an excellent approximation there. For $S \gg 1$, $(\lambda, \mu) \simeq (0.6, 0.5)$ and (4.13) is in good agreement with the time solution; for $S \ll 1$ this is not so.

The result (4.13) depends on assuming that the exponential profile is a good approximation for $0 < x < \infty$, but only at the moment of pool maximum. An alternative approach is to assume that the exponential profile is a good approximation in the vicinity of the melting front only, but at all times prior to pool maximum. In these circumstances (4.10) and (4.11) hold for all t, and eliminating $\delta$ we obtain

$$\frac{u}{\kappa}(1+S^{-1}) = \frac{bf}{r_o^2} - \frac{2}{r_o} \tag{4.15}$$

This is an ordinary differential equation for the position of the front as a function of time. This can be solved in a straightforward way using an ODE solver package, and this has been carried out in a computer program called SPHINX. Results for different values of S are shown in Table 1 and Figs. 8(a,b,c). The results correspond to

$$(\lambda_c, \mu_c) = \left(\left[1-2\int_{r_o}^{t_c} dt/b\tau\right]^{1/3}, \tfrac{1}{2}\right) \tag{4.16}$$

As the figures show, (4.15) models the time dependent change of $\lambda$ from 1 at early times towards the appropriate value at pool maximum quite well. The actual estimate of maximum pool radius $r_c$ based on SPHINX is significantly poorer ($\sim 10\%$ error) than the Ansatz estimate. The time error is smaller for $t_c$ at small S but much worse at large S.

## 4.4. The Exp-Erfc Profile

An alternative temperature profile which may be considered is

$$\theta = \frac{r_o}{r} \exp(-ux/\kappa)\,\mathrm{erfc}(x/2\sqrt{\kappa t}) \tag{4.17}$$

This tends to the 'fast melting front' solution (3.8) provided $\frac{\partial y}{\partial t}$ can be neglected in (3.7) and to the external solution for a fixed sphere of radius $r_o$,

when $u\frac{\partial y}{\partial x}$ can be neglected in (3.7).   (4.17) is not a solution of (3.7) but is a hybrid containing significant features of a true solution.

If it is now assumed that this profile is a good approximation in the vicinity of the melting front at all times prior to pool maximum, then the Stefan boundary condition (3.16) becomes

$$\frac{u}{\kappa}\left(1 + S^{-1}\right) = \frac{bf}{r_o^2} - \left(\frac{1}{r_o} + \frac{1}{\sqrt{\pi\kappa t}}\right) \qquad (4.18)$$

This ordinary differential equation is a modification of (4.14) and can be solved in the same fashion.  The solution is here called SPHINX II, and the corresponding radius and time of pool maximum are labelled $r_c'$ and $t_c'$. The values for the test problems are given in table 1.  The pool sizes are accurate to 5% for all values of S and the time of pool maximum accurate to better than 25%.  In view of the broad 'flat' nature of the maximum of $r_o(t)$, this estimate $t_c'$ for the time of pool maximum is satisfactory.  Unlike the exponential Ansatz, the exp-erfc profile gives more accurate results as S becomes small.  Figs. 8(a, b, c) also show the time development of the solution using the exp-erfc profile;  it follows the true solution much more faithfully than that generated by (4.15).

At pool maximum if we assume that (4.17) holds for $\theta < x < \infty$, then the enthalpy ratio $G = \left(\frac{S}{1+S}\right)\left(\frac{6}{\pi}\right)\left(\frac{\delta_\kappa}{r_o}\right)\left(1 - \frac{\delta_\kappa}{r_o}\right)$ where $\delta_\kappa = \sqrt{\pi\kappa t}$.  This has as its maximum value $\frac{12}{\pi}\left(\frac{S}{1+S}\right)$ which is a reasonable estimate for G when $S > 1$, but poor when $S \ll 1$.  Thus the profile (4.17) is good at approximating the local property $\frac{\partial\theta}{\partial x}\Big|_{x=0}$ at the melting front, and rather poor at approximating the integral property G.

## 4.5  A Special Case : $f = f_o t^{-\frac{1}{4}}$

The decay heating function $f = f_o t^{-\frac{1}{4}}$, besides being a good approximation to that for a nuclear reactor with heavily radiated fuel, is also a particularly simple case mathematically, for then $\tau = f_1^3 t^{\frac{3}{4}}$ where $f_1^3 \equiv 4f_o/3$.  Equations (4.2) and (4.3) become

$$\left. \begin{aligned} r_o &= af_1\, t^{\frac{1}{4}} \\ r_o &= bf_o\, t^{\frac{1}{4}} \end{aligned} \right\} \qquad (4.19)$$

which gives $r_B^2 = abf_o f_1$ ;   $t_B^{3/2} = \frac{3}{4}f_o^2(1+S)t_N = \left(\frac{bf_o}{af_1}\right)^3$

Correspondingly the Ansatz point A is given by $r_A = \sqrt{\lambda_A \mu_A}\ r_B$ ; $t_A = \left(\dfrac{\mu_A}{\lambda_A}\right)^2 t_B$

where $\lambda_A$ and $\mu_A$ are given by (4.13). One can show that the solution of (4.14) has the form $r_o = \mu b f$ where $\mu$ is a function only of $\left(\dfrac{t}{t_B}\right)$ and has a series expansion

$$\mu = \left(\frac{t}{t_B}\right)^{\frac{1}{2}}\left(1 - \frac{2}{5}\left(\frac{t}{t_B}\right)^{\frac{1}{2}} + \frac{8}{175}\left(\frac{t}{t_B}\right) + \right) \tag{4.20}$$

On the other hand (4.18) can be re-written when $f = f_o t^{-\frac{1}{4}}$ as

$$4\mu^2\left[\frac{d\mu}{d\sigma} - \frac{\mu}{4\sigma}\right] = \sigma^{\frac{1}{2}}\left[1 - \mu - \mu^2 \gamma \sigma^{-\frac{3}{4}}\right] \tag{4.21}$$

where $\sigma = \dfrac{t}{t_B}$ and $\gamma^2 = \dfrac{4}{\pi}\ \dfrac{S}{1+S}$ thus showing that $\mu$ has the functional dependence, $\mu = \mu(S, \dfrac{t}{t_B})$, in this case.

This example provides a good test case for the external one-phase Stefan problem, by means of which the effectiveness of different numerical methods in two or more dimensions can be assessed over the whole range of Stefan number. It can also be used to test two-phase codes by distributing the heat source within the pool and assigning a very high conductivity to the liquid phase. To avoid any starting problems, the small time solution $r_o = a\tau^{1/3}$ should be used.

## 4.6 Resumé

The analysis presented in this section (§4) can be summarized as follows:

(i) the maximum radius for a hemispherical cavity produced by decay heating can be approximated to within 3% by the algebraic formulae (4.13) and (4.14) over the whole range of Stefan numbers. The time of pool maximum can be estimated to much better than 50% by the use of (4.5). These formulae give this accuracy with 10 to 20 evaluations of the function $\tau/f^3$ which is assumed known, at least in tabular form.

(ii) Use of the exp-erfc profile (4.17) leads to a single ordinary differential equation for the position of the advancing front as a function of time. This ODE (4.18) follows the growth of the cavity for several years resulting in maximum pool sizes accurate to 5% for all values of S and times of pool maximum overestimated by less than 25%. Roughly 700 steps are required with $\sim 10^3$ evaluations of f and the r.h.s of (4.17). This is at least an order of magnitude cheaper than

4.6

solving (3.15)-(3.16) as a partial differential equation by any of the available methods, but of course the accuracy achievable is limited.
(iii) The heating source function $f = f_o t^{-\frac{1}{4}}$ provides a good test case for the external one-phase Stefan problem.

# 5.    MULTIDIMENSIONAL MELTPOOL FRONT TRACKING

In §3 and §4, the growth of meltpools has been considered when the pool shape and the temperature profile within the solid phase are radially symmetric. In practice, convection within the molten pool results in the heat flux at the liquid/solid interface being a function of position on that interface. The non-uniformity of the flux results in the pool shape and the temperature profile within the solid phase becoming dependent on all the spatial co-ordinates as well as time. A number of methods are available for computing such a system including the enthalpy method [9, 10], the method of lines [11], IMM [12, 13]  and co-ordinate transformation methods [14]. Turland has recently shown how to express the IMM transformation in orthogonal curvilinear co-ordinates [7] in an elegant 'flux conservation' form and this is the basis of a version of IMM in spherical polars in which the finite difference scheme can be put in conservative form. However the aim here is to find effective approximate methods in the absence of radial symmetry. Algebraic formulae analogous to (4.13) and (4.14) are not to be found, for the pool will reach its maximum extent at different times along different radial rays;  but  a set of first-order ordinary differential equations analogous to (4.13) or (4.18) could track the position of the melting front as a function of time.

Let $\underline{r}$ be the position vector, and $\underline{\hat{n}}(\underline{r})$ be the local normal to the isotherms so that the vector field $\underline{\hat{n}}$ represents the thermal flux lines. The metric $d\Sigma$ can be taken in the form

$$d\Sigma^2 = dn^2 + h_2{}^2 dv^2 + h_3{}^2 dw^2 \tag{5.1}$$

where $dn$ is the line element parallel to $\underline{\hat{n}}$ and $v$ and $w$ are some corresponding orthogonal curvilinear co-ordinates. The Fourier equation can then be recast in IMM form as

$$\frac{\partial n}{\partial t} = - \frac{\kappa}{h_2 h_3} \frac{\partial}{\partial \theta} \left( h_2 h_3 \left( \frac{\partial n}{\partial \theta} \right)^{-1} \right) \tag{5.2}$$

where $\theta$ is the dimensionless <u>temperature</u> and the derivatives are taken with $v$ and $w$ constant. The coefficients $h_2$ and $h_3$ are functions of position and $n$ is the distance along a flux line. Equation (5.2) is a specialization of Turland's general form [7], and carrying out the differentiation we obtain[†]

$$\frac{\partial n}{\partial t} = \kappa \left[ \frac{\partial^2 n}{\partial \theta^2} \left( \frac{\partial n}{\partial \theta} \right)^{-2} - \frac{1}{\rho} \right] \tag{5.3}$$

[†]Note that (5.3) is exact since n is the distance measured along a curvilinear flux line normal to successive isotherms (see fig. 10).

where $\rho$ is the total radius of curvature (which is the sum of the two principal curvatures) given by

$$\rho^{-1} = \text{div } \hat{n} = \frac{1}{h_2 h_3} \frac{\partial}{\partial n} (h_2 h_3)$$

in this metric. In strict spherical symmetry n=r and $\frac{1}{\rho} = 2/r$, so that we recover (3.14). For cylindrical symmetry $\frac{1}{\rho} = 1/r$ (cf [13]).

The Stefan condition is

$$\rho L \left. \frac{\partial n_o}{\partial t} \right|_{v, w} = Q_o \frac{g}{2\pi} + (k\Delta T) \left( \frac{\partial n}{\partial \theta} \right)^{-1}_{n=n_o} \tag{5.4}$$

where $(g/2\pi)$ is the heat flux from the pool to the melting front and is a function of time and position on the melting front. Thus $\int g\hat{n}.d\underline{S} = 2\pi f$. In terms of b and S, (5.4) becomes

$$\frac{\partial n_o}{\partial t} = \kappa S (bg + n_{\theta 0}^{-1}) \tag{5.5}$$

Equations (5.3) and (5.5) are exact and can be made the basis of an IMM numerical scheme in the same spirit as Crank and Crowley [13].

If the exponential Ansatz is assumed to hold locally in the vicinity of the melting front in the form

$$\theta = \exp(-x/\delta) \tag{5.6}$$

where $x = n - n_o$, (v, w, t) is the distance from the melting front measured down a flux line and $\delta$(v, w, t) satisfies

$$\frac{1}{\delta} = \left( \frac{1}{\kappa} \frac{\partial n_o}{\partial t} \right) + \frac{1}{\rho_o}$$

then (5.5) becomes

$$\frac{dn_o}{dt} = \frac{\kappa S}{1+S} (bg - \frac{1}{\rho_o}) \tag{5.7}$$

$\rho_o$ is the mean curvature at each point in the melting front and profile (5.6) satisfies the linearised equation $\theta_{nn} + \frac{1}{\delta}\theta_n = 0$. (cf 4.1). Knowing the current position of the melting front, the curvature and direction of the normals can be calculated, as can the appropriate flux function g from other studies of convection in pools [e.g. 15]. Hence (5.7) can be used to follow the advance of the front explicitly. Since only the meltpool front

is tracked, a large number of 'marker particles' can be used to ensure that curvature and normal directions are calculated accurately. In cylindrical polars $(r, \phi, z)$ for which $d\Sigma^2 = dr^2 + r^2 d\phi^2 + dz^2$, with azimuthal symmetry $(\frac{\partial}{\partial\phi} \equiv 0)$, the equations of motion for the $i^{th}$ 'marker particle' on the front are, for an explicit numerical scheme (dropping the zero subscript since all quantities are evaluated at the melting front),

$$
\left.
\begin{aligned}
dn_i &= \left(\frac{\kappa S}{1+S}\right) dt \, (bg(r_i, z_i) - \rho_i^{-1}) \\[2mm]
dr_i &= (\Delta z_i)(dn_i)/(\Delta s_i) \\[2mm]
dz_i &= (\Delta r_i)(dn_i)/(\Delta s_i)
\end{aligned}
\right\}
\tag{5.8}
$$

where $dn_i = n_i(t+dt) - n_i(t)$ etc, $\Delta r_i = r_{i-1} - r_{i+1}$, $\Delta z_i = z_{i+1} - z_{i-1}$, $(\Delta s_i)^2 = (\Delta r_i)^2 + (\Delta z_i)^2$, and

$$
\rho_i^{-1} = \frac{\Delta z_i}{r_i \, \Delta s_i} + 2 \frac{(\Delta r_i)^2}{(\Delta s_i)^3} \left[ \frac{z_{i+1} - z_i}{r_{i+1} - r_i} - \frac{z_i - z_{i-1}}{r_i - r_{i-1}} \right]
\tag{5.9}
$$

Equation (5.7) can be modified as (4.15) was modified into (4.18) to give

$$
\frac{dn_o}{dt} = \frac{\kappa S}{1+S} \left( bg - \left[ \frac{1}{2\rho_o} + \frac{1}{\sqrt{\pi \kappa t}} \right] \right)
\tag{5.10}
$$

which can be used to track the melt front in the same way as (5.7) by appropriate changes to (5.8). Whether (5.7) or (5.10) is more accurate in the absence of radial symmetry has not yet been properly assessed.

# 6.    STABILITY

In considering the advance of a molten pool into a solid substratum, or the melting of support structures by overlying hot debris, it is usually assumed that the advancing melt front is a plane or simple curved surface. Penetration times based on this assumption would be overestimated if the melting front were unstable to small spatial variations in the temperature distribution, as then the interface could become very convoluted, leading to increased local penetration and possible structural failure.

We consider here the linear stability analysis for a plane melting front advancing steadily at velocity u into a solid as a result of a high heat flux $\Phi$ being applied to the liquid phase, normal to the front. The liquid phase is assumed to overly the solid phase so that the liquid phase is thermally stratified and stable against Bénard convection. In the frame of reference $(x, y, \chi)$ moving with the front, the solid has velocity $-u_s = -u$. After melting, the liquid moves away from the front with velocity $- u_L$, where from mass conservation $\rho_s u_s = \rho_L u_L$ ($\rho_s$ solid density, $\rho_L$ liquid density). For two semi-infinite plane layers the mean temperature profiles are

$$T_0 (\chi) = T_s [\exp(-u_s\chi/D_s) - 1] \qquad (\chi > 0 : \text{solid})$$
$$= T_L [\exp(-u_L\chi/D_L) - 1] \qquad (\chi < 0 : \text{liquid}) \tag{6.1}$$

where the melting temperature is taken as zero, the ambient temperature in the solid is $-T_s$ (as $\chi \to \infty$) and $T_L \equiv (c_s T_s + L)/c_L$. Also $D_s$ and $D_L$ are the respective thermal diffusivities.

Provided $|\chi| \ll D_L/u_L$, the mean temperature profile in the liquid approximates to the linear profile $- \Phi\chi/k_L$. The solution becomes infinite as $\chi \to -\infty$ and so some cut-off is appropriate. Physically this is consistent with a source of heat flux $\Phi$ at some fixed distance from the melting front; essentially this is a case for a well mixed pool separated from the melting front by a thermal boundary layer.

A spatial perturbation $\xi = \xi_0 \exp(imx - \alpha t)$ at the melting front leads to corresponding temperature perturbations $\hat{\theta} = g(\chi) \exp(imx - \alpha t)$, assuming $\frac{\partial}{\partial y} \equiv 0$. From the linearized Navier-Stokes (including viscosity) the $\chi$-component of velocity has the form $v_\chi = h(\chi) \exp(imx - \alpha t)$ where

$$h(\chi) = v_0 \exp(m\chi) + v_1 \exp(m_1\chi)$$

in which $m_1{}^2 = m^2 - (\alpha/\nu)$ where $\nu$ is the kinematic viscosity of the liquid.

When the temperature equation, the Navier-Stokes equation for the liquid and the boundary conditions (viz. (i) continuity of temperature (ii) the Stefan condition (iii) the no-slip condition) are combined together in linearized form to eliminate the amplitudes of the linear perturbation, the following dispersion relation results

$$L\, bm\gamma + (1-L)n_s{}^* + n_L{}^* + \frac{\gamma(b-1)}{m_1-m} \left[\frac{m_1(n_L{}^*-m^*)}{\gamma+1} - \frac{m(n_L{}^*-m_1{}^*)}{\gamma(1-\sigma^{-1})+m_1/m}\right] = 0 \qquad (6.2)$$

where b is the density ratio $\rho_s/\rho_L$ and $L$ is the modified Stefan number $L/(c_L T_L)$. Also $\sigma$ is the Prandtl number $(\nu/D_L)$, $\gamma$ is the dimensionless growth rate $-\alpha/mu_L$, $m^* = m-u_L/D_L$, $m_1{}^* = m_1-u_L/D_L$ and $n_L{}^*$ and $n_s{}^*$ are given by

$$n_s{}^* = u_s/2D_s + (u_s{}^2/4D_s{}^2 + m^2 - \alpha/D_s)^{\frac{1}{2}}$$

$$n_L{}^* = -u_L/2D_L + (u_L{}^2/4D_L{}^2 + m^2 - \alpha/D_L)^{\frac{1}{2}}$$

For perturbations which decay spatially as $|\chi| \to \infty$, it is necessary that

$$\mathrm{Re}(n_s{}^*) > 0, \ \mathrm{Re}(n_L{}^*) > 0, \ \mathrm{Re}(m_1) > 0, \ \mathrm{Re}(m_1{}^*) > 0, \ m > 0, \ m^* > 0. \qquad (6.3)$$

The dispersion relation (6.2) has been examined numerically subject to these constraints for ranges of Prandtl number, Stefan number, density ratio and horizontal wavenumber, and all such localized modes are found to decay with time. When viscosity is zero, Peckover and Turland [16] have proved rigorously that such localized modes are stable. When liquid and solid phases have equal densities, the dispersion relation reduces to

$$L\, bm\gamma + (1-L)n_s{}^* + n_L{}^* = 0$$

and $\mathrm{Re}(\gamma) > 0$ by inspection.

When $u \to 0$, the unperturbed temperature profile becomes piecewise linear, and the decay rate $\alpha$ becomes real and has the explicit form

$$\alpha = u_T{}^2\{2([m/u_T]^2 + D_L{}^{-1}D_s{}^{-1})^{\frac{1}{2}} - (D_L{}^{-1} + D_s{}^{-1})\}$$

where $u_T = \Phi/\rho_s L$ is the speed at which the melting front would advance into a solid already at its melting point.

6.2

The influence of constant temperature or constant flux boundaries at a finite distance from the melting front has also been examined [16, 17]. The placement of the boundary conditions closer to the melting front enhances stability.

The conditions (6.3) mainly determine which sign is taken for a square root, however $m^* > 0$ implies $m > u_L/D_L$ i.e. the horizontal wavelength must be sufficiently short that the thermal diffusion speed $mD_L$ exceeds the flow velocity $u_L$ away from the melt front in the liquid. If this condition is not satisfied such a Fourier mode will not be spatially localised.

The dispersion relation if of some mathematical interest. It usually has two branches, one of which is completely unstable and the other is stable except for small wavenumbers. The spatial structure of a mode of the form $\exp(imx - \alpha t)$ is always the sum of terms of the form $\exp(N\chi)$ where N can be complex. Spatially localised modes have $\text{Re}(N) < 0$ when $\chi > 0$ and $\text{Re}(N) > 0$ when $\chi < 0$ and these can satisfy boundary conditions which dictate decay in spatial amplitude as $|\chi| \to \infty$. Other possible modes of the dispersion relation are those that oscillate indefinitely in space in the $\chi$-direction, and spatially explosive modes whose amplitudes become infinite as $|\chi| \to \infty$; some of these latter modes are stable and some unstable, but all must be excluded if the boundary conditions at infinity are rigorously applied. The spatially localised modes are all stable. It would be of interest for this linear stability problem to be imbedded in a more general formulation where perhaps the power of functional analysis could be utilised.

# 7.    CONCLUSION

Stefan problems arise in a number of circumstances considered in reactor safety studies.   The growth of a molten pool in a solid has been considered in some detail and approximate methods of tracking the movement of the melting front devised.   Detailed comparisons have been made for a wide range of Stefan numbers in the case of spherical symmetry between results from full solutions and those obtained by approximate methods.   The comparisons suggest that these approximate methods may be effective in multidimensional problems. The heat source function $f=f_o t^{-\frac{1}{4}}$ provides a useful model problem for the external one-phase Stefan problem.   The stability of the shape of a melting front against the development of ripples or fingers is an important practical problem;   the results of a linear stability analysis for a plane interface are  discussed.

REFERENCES

[1]  Stefan J (1891) Ann Phys u. Chem 42 269-286

[2]  Peckover R S, Turland B D and Whipple R T P (1977). On the Growth of
     Melting Pools in Sacrificial Materials in Proc. Third Post Accident Heat
     Removal Conf. Argonne Nat. Lab. Chicago Nov 1977 (also UKAEA Culham
     Report CLM-P511)

[3]  Way K and Wigner E P (1948) Phys. Rev. 70, 138

[4]  Fox L (1975) What are the best numerical methods? in Moving Boundary
     Problems in Heat Flow and Diffusion (Ockenden J R and Hodgkins W R,
     editors) Clarendon Press, Oxford p210 ff.

[5]  Dix R C and Cizek J (1971) The isotherm migration method for transient
     heat conduction analysis Proc. Fourth Int. Heat Transfer Conf. Paris
     Vol I A.S.M.E. (N.York)

[6]  Crank J and Phahle R D (1973) Bull I M A 9, 12.

[7]  Turland B D (1978) Conservative Isotherm Migration Method for Stefan
     Problems. Paper presented at the Symposium on 'Free and Moving Boundary
     Problems in Heat Flow and Diffusion' Durham July 1978

[8]  Acton F S (1970) Numerical Methods that work. Harper-Row N.York p 52 ff.

[9]  Meyer G H (1973) Multidimensional Stefan Problems. SIAM J. Numerical
     Anal. 10, 522-238.

[10] Crowley A B (1978) Numerical solution of Stefan problems Int. J. Heat
     Mass Transfer 21, 215-217.

[11] Meyer G H (1976) The Numerical Solution of Stefan Problems with Front
     Tracking and Smoothing Methods. Brunel Report TR/62.

[12] Crank J and Gupta R S (1975) Isotherm migration method in two dimensions
     Int. J. Heat Mass Transfer 18, 1101-1107

[13] Crank J and Crowley A B (1978) Isotherm Migration along orthogonal flow
     lines in two dimensions. Int. J. Heat Mass Transfer 21, 393-398.

[14] Furzeland R M (1977) Numerical Solution of Two-dimensional Moving
     Boundary Problems using Curvilinear Co-ordinate Transformations. Brunel
     Report TR/77.

[15] Jahn M and Reineke H H (1974) Free Convection Heat Transfer with internal
     heat sources: calculations and measurements Proc. 5th Int. Heat Transf.
     Conf. Tokyo.

[16] Turland B D and Peckover R S (1978) The Stability of Planar Melting Fronts
     in 2-Phase Thermal Stefan Problems. J.Inst. Math. Appl. (In Press).

[17] Turland B D, Peckover R S and Dullforce T A (1977) On the Stability of
     Advancing Melting Fronts to Spatial Perturbations in Proc. Third Post
     Accident Heat Removal Conf. Argonne Nat. Lab. Chicago Nov 1977. (Also
     UKAEA Culham Report CLM-P512).

## Acknowledgements

## MAXIMUM POOL SIZE

| $S \equiv \frac{c \Delta T}{L}$ | $\log t_N$ | ISOTHM<br>Point M | Point B | Ansatz<br>Point A | SPHINX I<br>Point C | SPHINX II<br>Point C' |
|---|---|---|---|---|---|---|
| 0.04 | 16.1 | $r_m = 10.67$ m<br>$t_m = 8.34 \times 10^8$ s | $r_B = 1.32\ r_m$<br>$t_B = 0.93\ t_m$ | $r_A = 1.03\ r_m$<br>$t_A = 0.35\ t_m$ | $r_C = 0.88\ r_m$<br>$t_C = 0.50\ t_m$ | $r_C' = 1.02\ r_m$<br>$t_C' = 1.13\ t_m$ |
| 2.10 | 14.4 | $r_m = 16.10$ m<br>$t_m = 1.45 \times 10^8$ s | $r_B = 1.66\ r_m$<br>$t_B = 1.26\ t_m$ | $r_A = 0.99\ r_m$<br>$t_A = 0.80\ t_m$ | $r_C = 1.05\ r_m$<br>$t_C = 0.66\ t_m$ | $r_C' = 1.04\ r_m$<br>$t_C' = 1.16\ t_m$ |
| 105 | 12.9 | $r_m = 16.55$ m<br>$t_m = 1.07 \times 10^8$ s | $r_B = 1.75\ r_m$<br>$t_B = 1.38\ t_m$ | $r_A = 0.98\ r_m$<br>$t_A = 1.03\ t_m$ | $r_C = 1.10\ r_m$<br>$t_C = 0.73\ t_m$ | $r_C' = 1.05\ r_m$<br>$t_C' = 1.22\ t_m$ |

## TABLE I

The True Maximum Pool Size M and the Estimates B, A, C, C'
are also shown on Figures 8 (a-c).
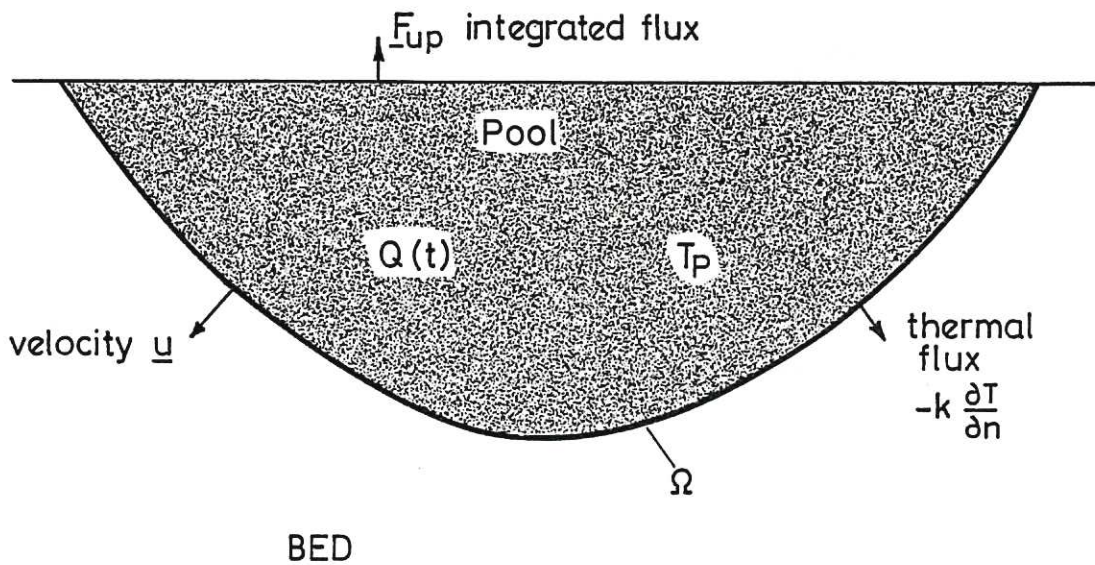
Fig.1 The melt pool. Its bulk temperature is $T_p$ and it contains distributed heat sources giving a spatially integrated heat source Q(t). A total thermal flux $F_{up}$ is transferred upwards. The lower surface of the pool $\Omega$ is advancing at a velocity $\underline{u}(\underline{r}, t)$.
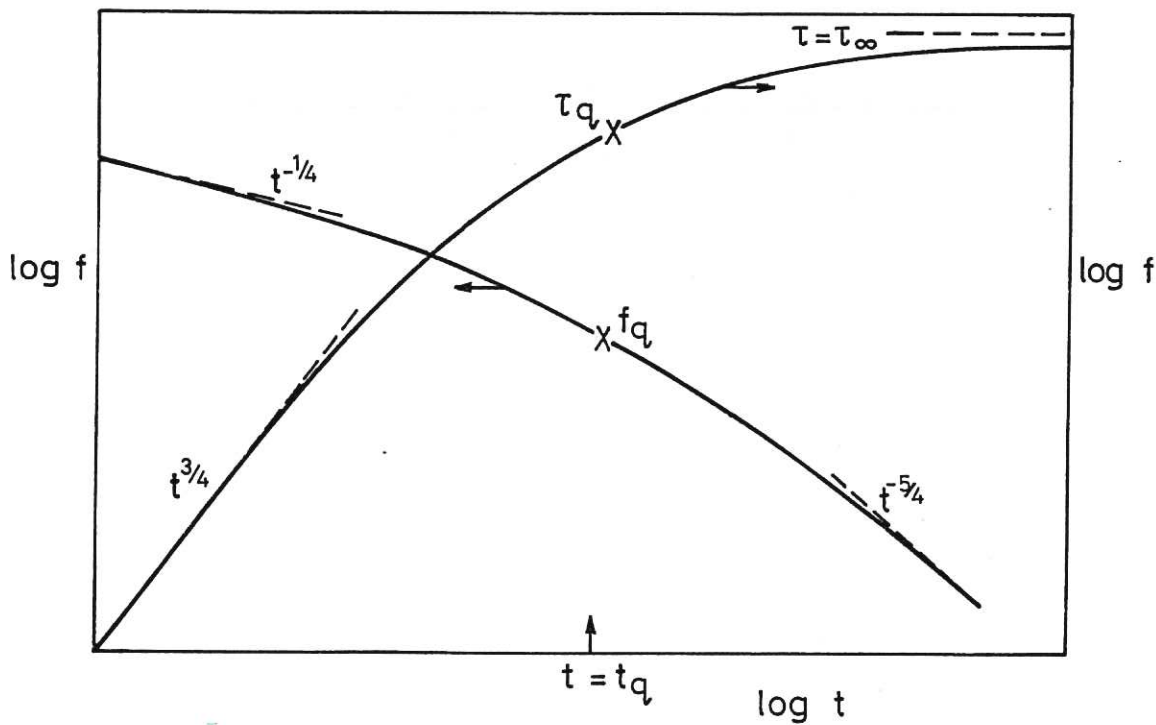


Fig.2 The decay heat function f and the integrated decay heat function $\tau$ as functions of time t when f is given by eq.(2.4) with $\alpha = \frac{1}{4}$. The irradiation time is $t_q$. For $t \ll t_q$, $f = f_0 t^{-\frac{1}{4}}$ and $\tau = 4f.t/3$. At $t = t_q$, $f = f_q \equiv \gamma_0 f_0 t_q^{-\frac{1}{4}}$ and $\tau = \tau_q \equiv 8f_q t_q/3$ where $\gamma_0 = (1-2^{-\frac{1}{4}}) = 0.16$.
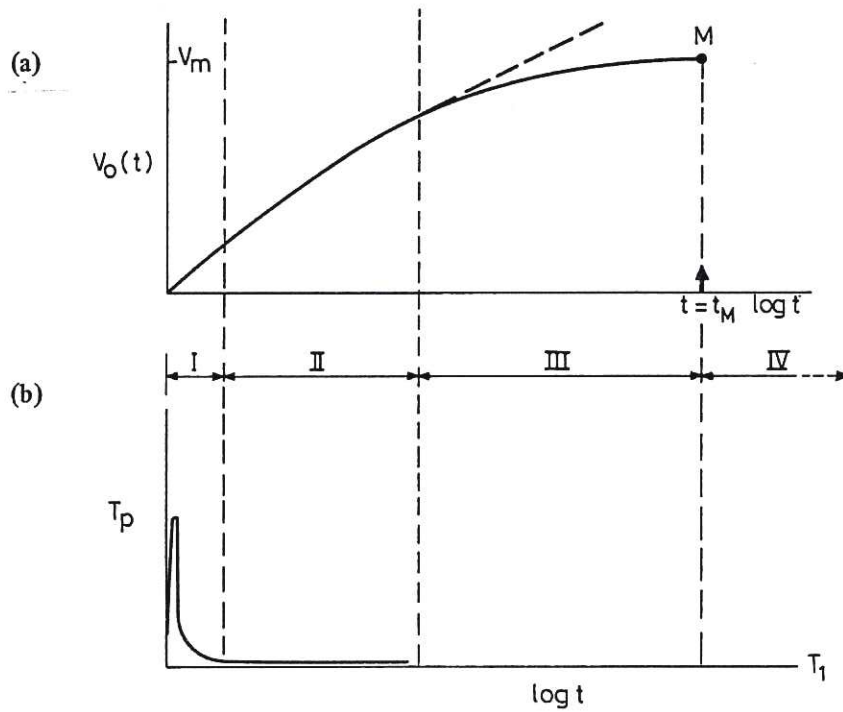
Fig.3 Schematic diagram of pool evolution showing the four temporal phases of §2.2. (a) Pool volume $V_0$ as a function of t. The point M at point $t_m$ represents the maximum pool volume $V_m$. The dashed line ----- indicates pool growth when thermal leakage is negligible. (b) Bulk pool temperature $T_p$ as a function of time, showing that its difference from $T_1$ is only significant in phase I.
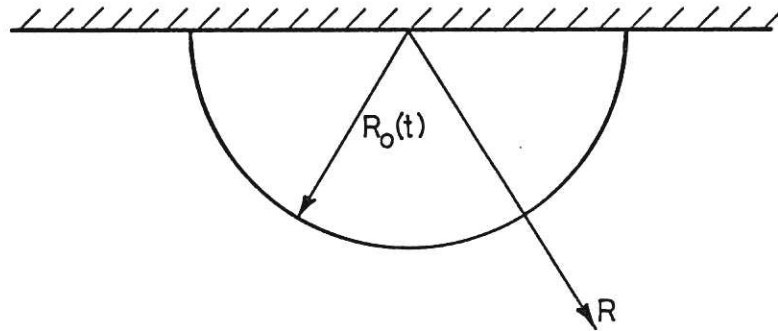


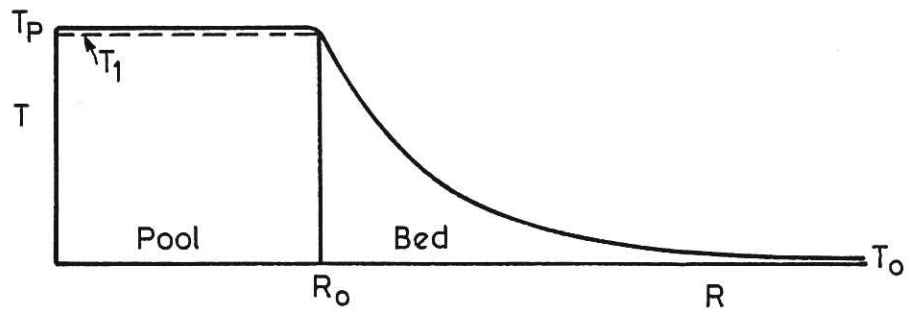Fig.4(a) Hemispherical pool of radius $R_0(t)$, with adiabatic lid.



Fig.4(b) Corresponding temperature profile as a function of radius R. $T_0$ is the ambient temperature of the bed and $T_1$ is its melting point; $T_p$ is the bulk temperature of the pool.
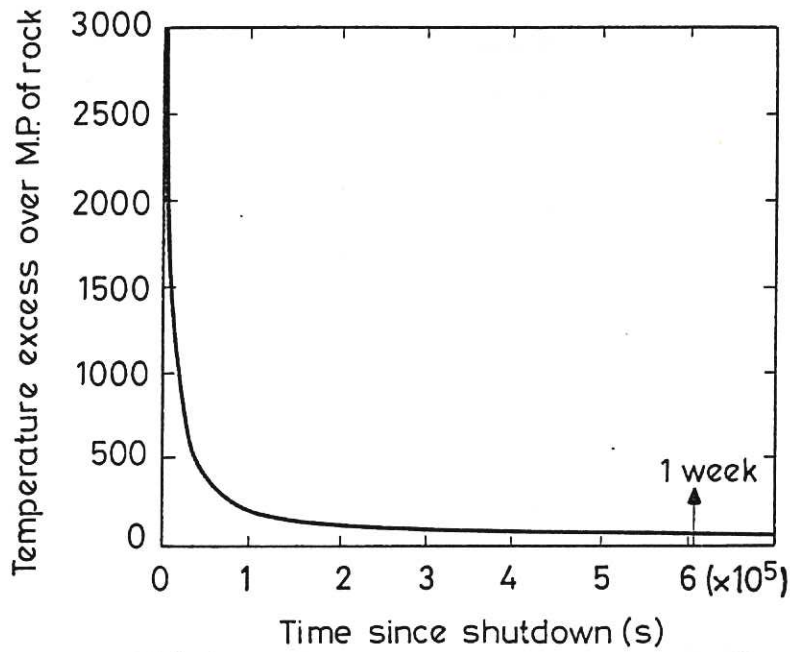
Fig.5 Bulk temperature of a hemispherical pool as a function of time calculated using the Whipple eq.(3.6). In the example, the initial pool temperature is 1500 K above the melting point and rises rapidly before decaying, as shown.
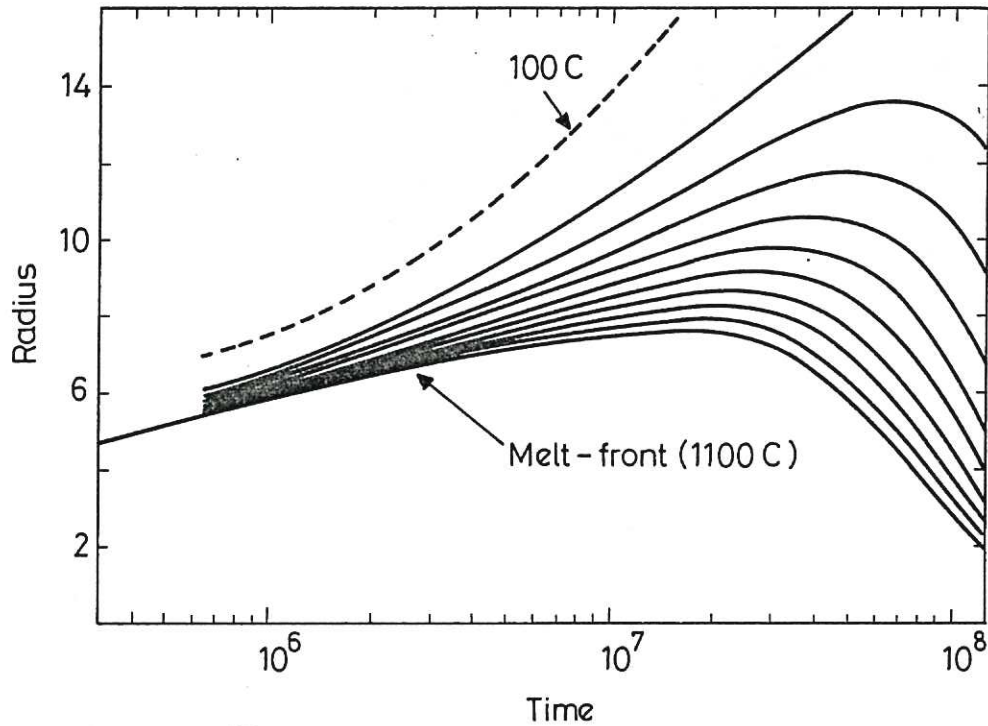


Fig.6 The evolution of isotherms as a function of time $t$ calculated by the ISOTHM program when $S \sim 2$. The lowest isotherm in the figure shows the location of the hemispherical melt front reaching a maximum radius, followed by pool contraction. The remaining isotherms shown are equally spaced in temperature. The dashed isotherm is essentially at ambient temperature; beyond it, the presence of the melt pool has a negligible influence on the temperature of the bed material.
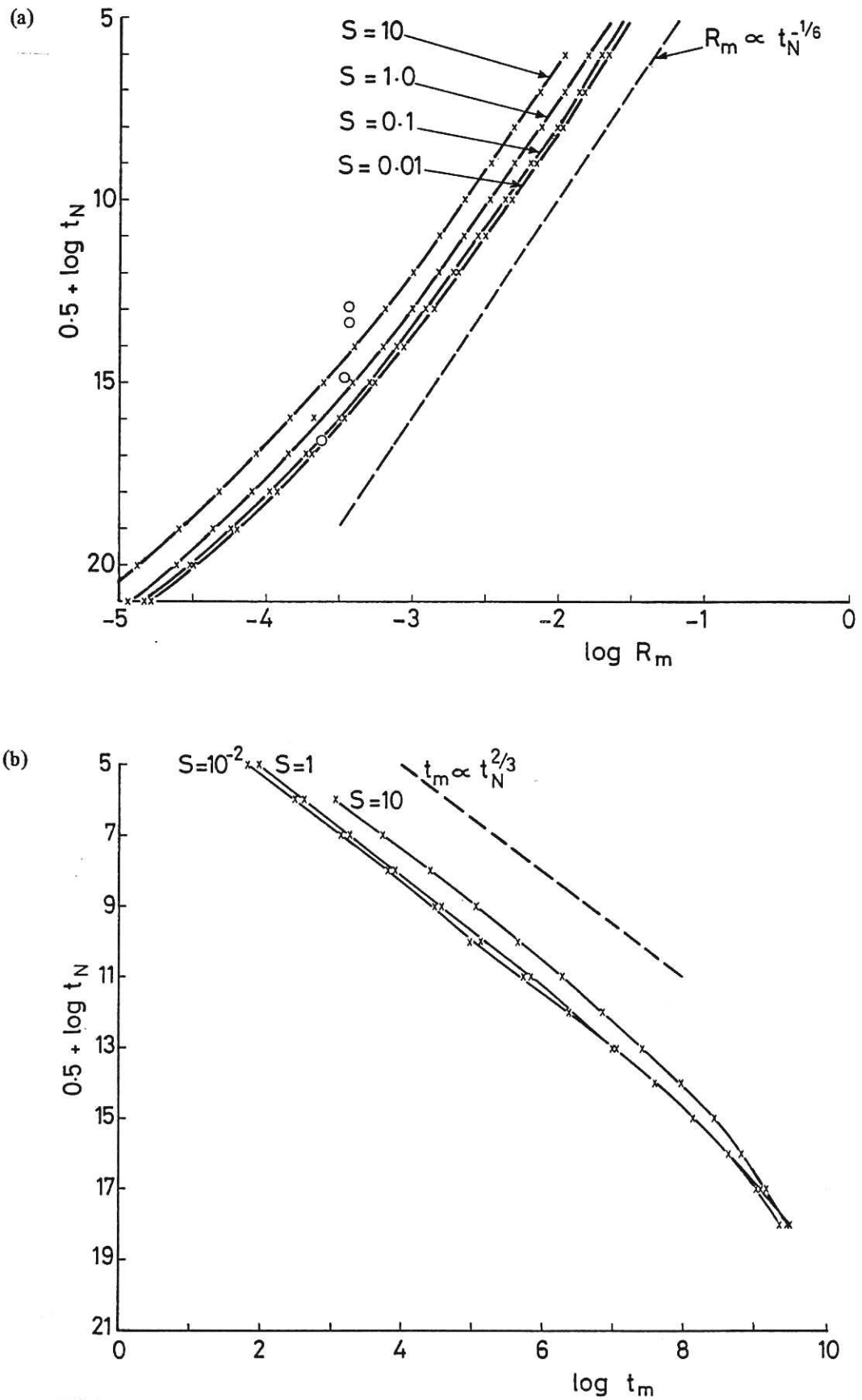
Fig.7 (a) the dimensionless maximum pool radius $R_m$ and (b) the corresponding time $t_m$ as functions of the two independent parameters that define the system viz the Stefan number S and the timescale $t_N$ (eq.3.10). The irradiation time $t_q$ is chosen to be $10^{10}$ sec and $a = \frac{1}{4}$ in eq.(2.4). When $t_m \ll t_q$, then $R_m \propto t_N^{-\frac{1}{6}}$ and $t_m \propto t_N^{\frac{2}{3}}$; these gradients are shown by dashed lines.
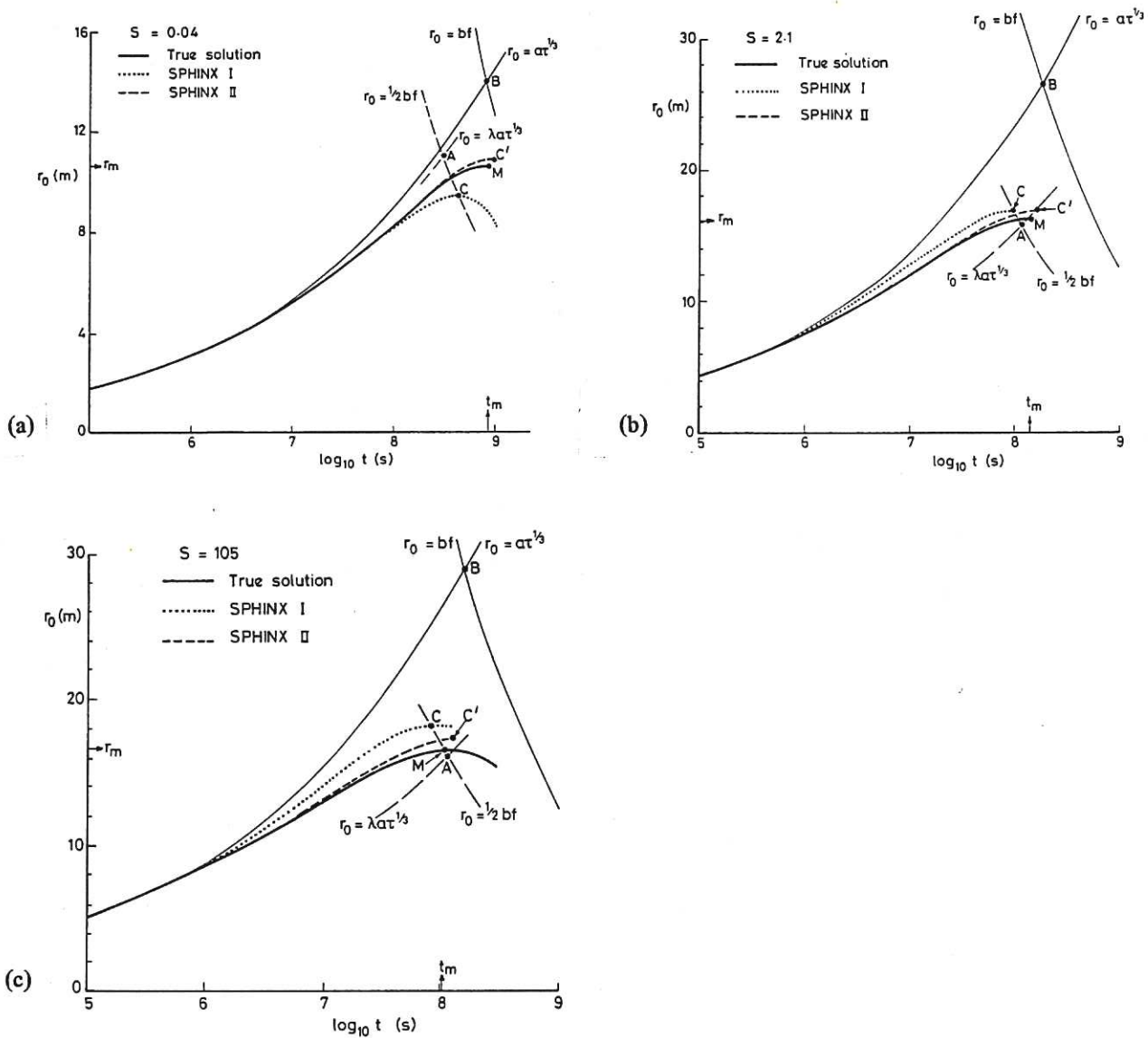
Fig.8 The growth of the radius $r_0$ of a hemispherical melt-pool as a function of time t for three different values of the Stefan number S viz (a) 0.04, (b) 2.1, (c) 105. In each case, the true solution is represented by a heavy line ————, the solution calculated by SPHINX I (eq.4.14) by . . . . . . . ., and that calculated by SPHINX II (eq.4.17) by - - - - - -; the corresponding maximum pool sizes occur at M, C and C′ respectively. The bounding curves (4.2) and (4.3) are given by thin solid curves ————, and their intersection is the point B. The Ansatz estimate of maximum pool radius (eq.4.12 and 4.4) is given by point A.
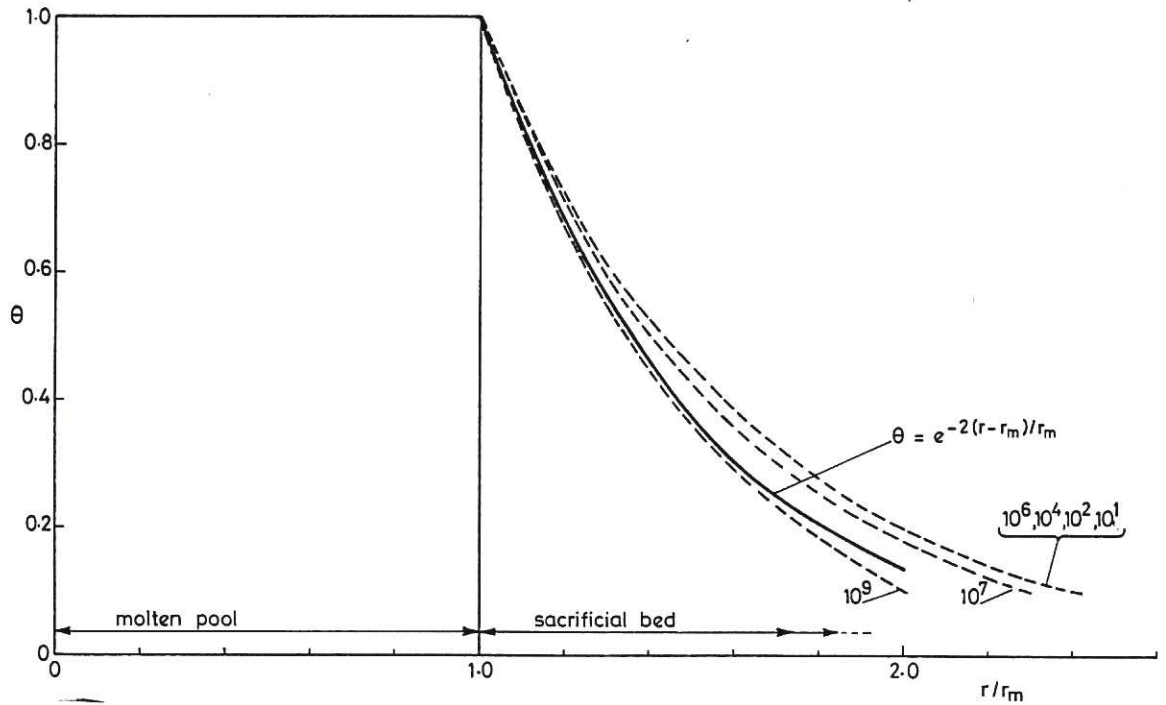
Fig.9 The dimensionless temperature $\theta$ as a function of r at the time of pool maximum; $r_m$ is the pool radius. The dashed lines show the profiles calculated using the ISOTHM program for a range of different values of $Q_o$ for $t_q = 10^{10}$ sec $S^{-1} \approx 0$. The solid line is the profile $\theta = \exp(-x/\delta)$ where $x = r-r_m$ and $\delta = \frac{1}{2}r_m$ (see §4.3).
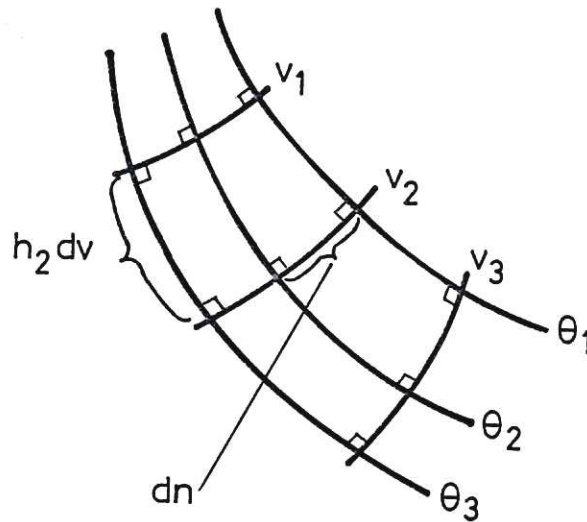


Fig.10 Orthogonal co-ordinates system showing 3 isotherms (lines of constant $\theta$) and 3 flux lines (lines of constant v). The third co-ordinate w is locally normal to the plane of the paper. The line element dn and its integral n are measured along the curvilinear flux lines. The mesh is convected with the motion which is always down instantaneous flux lines.